Jun-yao Wang ✉
Qi Hou
Fu-wang Wang
Bo You
Heng-yi Yuan

https://doi.org/10.21278/TOF.453009319
ISSN 1333-1124
eISSN 1849-1391

SIMULATION AND ANALYSIS OF THE HEATING PERFORMANCE OF AN EMBOSSING HEAD UTILIZING ELECTROMAGNETIC INDUCTION HEATING

Summary

In this paper, the embossing head of a hot embossing machine which uses the electromagnetic induction heating is studied. In order to determine the relevant performance parameters of the embossing head, i.e. the coil distribution position, material of the embossing head, heating frequency, cooling water velocity, simulation and analysis are carried out based on the finite element method in ANSYS/Workbench. The results demonstrate that a distance of 1 mm between the coil and the embossing head, copper as the embossing head material, a frequency of 8500Hz, and a water velocity of 1.2 $m \cdot s^{-1}$ satisfy the requirements, including those of a hot-pressing temperature of 150℃ and a demoulding temperature of 60℃. Simultaneously, the chip processing-cycle exploiting this embossing head is reduced by a factor of three. Compared with the existing heating methods of embossing heads, the electromagnetic induction heating method presented in this paper has the advantages of high efficiency, high heating rate, and long life.

Key words: *Simulation and analysis, Heating performance parameters, Embossing head, Electromagnetic induction heating, ANSYS*

1. Introduction

The microfluidic chip [1] with a microchannel structure and other functional units have been widely used in some fields, such as DNA analysis [2], immunoassays and food inspection, due to its main characteristics of rapidity, high effectiveness and low consumption [3]. Compared with glasses and silicon wafers, polymer materials [4] have the advantages of low price, simple manufacturing process, and good repeatability for chip fabrication. Furthermore, the polymer materials are classified into two categories: the thermosetting polymers such as polydimethylsiloxane (PDMS), [5], and the thermoplastic polymers such as polymethylmethacrylate (PMMA), [6]. Specifically, the thermoplastic materials offer higher impact strength, corrosion-resistance, and easy processing with better flow features for moulding complex designs than thermosetting materials [7]. The hot embossing machine with

superior properties of simple operation, steady running, and high automation degree [8] is the key equipment for the complete channel forming and packaging of thermoplastic materials [9,10].

Traditionally, two primary heating techniques, the resistance wire heating and the thermoelectric refrigeration reactor, are adopted in the hot embossing machine. For instance, a hot embossing machine with the resistance wire heating was established in [11] to manufacture the microfluidic chip. Nevertheless, the low thermal efficiency and short service life are the bottlenecks of this heating method. By comparison, a hot embossing machine utilizing a thermoelectric refrigeration reactor was employed to compensate for the insufficiency of the former method [12]. Unfortunately, in this method, 30% of the heat is not being utilized efficiently. Noticeably, the electromagnetic induction heating has the advantages of high efficiency, high heating rate, and long life [13]. Particularly, the heat transfer efficiency of this method can reach 90%; consequently, it has been introduced extensively into national defence, mechanical processing, and other fields. Thus, the electromagnetic induction heating technique was applied in a large-scale plastic processing system for solving the issues of high energy consumption and serious pollution [14]. However, the characteristics of high efficiency and stable operation are not specifically referenced in that system. Remarkably, the electromagnetic induction heating technique was utilized to implement the high efficient and stable operation of the heating system [15]. Nonetheless, the peculiarity of low sensitivity is neglected. Fortunately, the plastic-mould heating system [16] was ameliorated by using the electromagnetic induction heating method, and the requirements of strong controllability and high sensitivity were satisfied. To sum up, various performance advantages of electromagnetic induction heating technology have been gradually fully reflected in different equipment. Nevertheless, up to this point, no literature about a hot embossing machine utilizing the electromagnetic induction heating technology for manufacturing micro-structures has been reported.

In this paper, the embossing head of a hot embossing machine with the electromagnetic induction heating is utilized. The magnetic-thermal coupling field [17] of embossing head was simulated and analysed [18] in ANSYS/Workbench[19] to determine the relevant performance parameters of embossing head, i.e. the coil distribution, embossing head material, heating frequency, and circulating water velocity.

2. Theory of Research Method

2.1 Establishment of Mathematical Models

(1) Mathematical model of the electromagnetic field

The space distribution of electromagnetic field is described by Maxwell's equations (governing equation) including the Ampere circuital law, Faraday law of electromagnetic induction, Gauss law of electric flux, and Gauss law of magnetic flux; the differential forms are as follows:

$$\nabla \times \vec{H} = \vec{J} + \frac{\partial \vec{D}}{\partial t} = \vec{J}_s + \vec{J}_e + \frac{\partial \vec{D}}{\partial t} \tag{1}$$

$$\nabla \times \vec{E} = -\frac{\partial \vec{B}}{\partial t} \tag{2}$$

$$\nabla \times \vec{D} = \rho \tag{3}$$

$$\nabla \times \vec{B} = 0 \tag{4}$$

Where ∇, $\vec{H}$, $\vec{J}$, $\vec{J}_s$, $\vec{J}_e$, $\vec{D}$, $\vec{E}$, $\vec{B}$ and ρ are respectively the Hamiltonian; the magnetic intensity vector, A/m; the total density vector of conduction current, A/m^2; the density vector of source current, A/m^2; the density vector of induced eddy current, A/m^2; the vector of electric flux density, C/m^2; the electric intensity vector, v/m; the magnetic intensity vector, T; and the charge density, C/m^3.

The vectors $\vec{B}$, $\vec{H}$, $\vec{D}$, $\vec{E}$ satisfy the following relations:

$$\vec{B} = \mu \vec{H} \tag{5}$$

$$\vec{D} = \varepsilon \vec{E} \tag{6}$$

Where μ and ε are respectively the magnetic permeability, H/m, and the permittivity, F/m.

Generally, the current frequency range of induction heating is from medium to low frequency. Under this condition, the density amplitude of displacement current can be ignored because it is much smaller than the amplitude of the conduction current. Then, the formula (1) can be simplified as:

$$\nabla \times \vec{H} = \vec{J} = \vec{J}_s + \vec{J}_e \tag{7}$$

(2) Mathematical model of temperature field

For the induction heating process, the induced eddy current is equivalent to the internal heat source of the heated body, and the heat inside the heated body is transferred by the method of heat conduction. Assuming that the material properties of the heated body are isotropic, the governing equation is:

$$\rho c \frac{\partial T}{\partial t} = \lambda \left(\frac{\partial^2 T}{\partial^2 x} + \frac{\partial^2 T}{\partial^2 y} + \frac{\partial^2 T}{\partial^2 z} \right) + q \tag{8}$$

Where ρ, c, T, λ, and q are respectively the material density, kg/m^3; the specific heat capacity, J/kg℃; the temperature, ℃; the thermal conductivity, W/m℃; and the internal heat source generated by an eddy current, W/m^3.

The internal heat source q is generated through the per-unit volume heating of the induced eddy current, so it is expressed as follows:

$$q = J_e^2 / \sigma \tag{9}$$

Where σ is the electrical conductance, s/m.

(3) The calculation method of coupling field

The finite element method [20] is generally utilized for the numerical simulation of the electromagnetic-thermal coupling field. There are two methods for coupling the calculation of multi-physical field in the ANSYS, i.e. sequential coupling and direct coupling [21]. The sequential coupling method is used to perform two or more iterative analyses in sequence; it takes the analysis results of the previous field as the load of the latter field analysis so as to realize the coupling between multiple fields. The direct coupling method utilizes the coupling element type that contains all the necessary degrees of freedom to obtain the analysis result of

the coupling field only by solving it once. However, this method requires a higher computer configuration and a lower calculation efficiency.

In this paper, the sequential coupling method was employed based on the ANSYS/Workbench software [22] to accomplish magneto-thermal coupling analysis of the embossing head [23].

2.2 Calculation of Heat Transfer Efficiency

Heat transfer efficiency, as an important parameter in this study, is defined as the ratio of the actual heat transfer Q_A to the theoretical heat transfer Q_T; the difference between the two is due to the heat loss in the process of heat transfer. For electromagnetic induction heating, the heat loss mainly includes the coil loss $Q_1 = I^2 R$ and the heat conduction loss $Q_2 = \alpha\left(T - T_\alpha\right)$. The theoretical heat transfer is calculated using the formula (10) as follows:

$$Q_T = \frac{0.24\mu^2 N^2 S^2}{R^2 + X^2}\left(\frac{\mathrm{d}H(t)}{\mathrm{d}t}\right)^2 Rt \tag{10}$$

Where μ, N, S, R, X, and H are respectively the magnetic permeability, H/m; the coil turns; the area, m^2; the resistance of eddy current loop, Ω; the inductance of eddy current loop, Ω, and the magnetic intensity, A/m.

The actual heat transfer is calculated by the formula (11) as follows:

$$Q_A = Q_T - Q_1 - Q_2 \tag{11}$$

Consequently, the heat transfer efficiency ε is calculated by the formula (12) as follows:

$$\begin{aligned}\varepsilon &= \frac{Q_A}{Q_T} = \frac{Q_T - Q_1 - Q_2}{\dfrac{0.24\mu^2 N^2 S^2}{R^2 + X^2}\left(\dfrac{\mathrm{d}H(t)}{\mathrm{d}t}\right)^2 Rt} = \frac{\left(R^2 + X^2\right)\left(Q_T - Q_1 - Q_2\right)}{0.24\mu^2 N^2 S^2\left(\dfrac{\mathrm{d}H(t)}{\mathrm{d}t}\right)^2 Rt} \\ &= \frac{\left(R^2 + X^2\right)\left(\dfrac{0.24\mu^2 N^2 S^2}{R^2 + X^2}\left(\dfrac{\mathrm{d}H(t)}{\mathrm{d}t}\right)^2 Rt - Q_1 - Q_2\right)}{0.24\mu^2 N^2 S^2\left(\dfrac{\mathrm{d}H(t)}{\mathrm{d}t}\right)^2 Rt} \\ &= 1 - \frac{\left(R^2 + X^2\right)\left(Q_1 + Q_2\right)}{0.24\mu^2 N^2 S^2\left(\dfrac{\mathrm{d}H(t)}{\mathrm{d}t}\right)^2 Rt}\end{aligned} \tag{12}$$

It is to be noted that the heat efficiency boosts with increasing magnetic permeability. Remarkably, this further proves the advantages of choosing copper in this study because of its high magnetic permeability. Similarly, the heat transfer efficiency can be improved by increasing the coil turns and the area.

3. Simulation Process

The Maxwell 3D and Transient Thermal in the ANSYS/Workbench software were employed to accomplish the magneto-thermal coupling analysis of the embossing head.

(1) Model establishment

To meet the technological requirements for the manufacturing of polymer microfluidic chips, a model of embossing head is established, as shown in Figure 1. The thickness and diameter of the embossing head plate are 10 mm and 140mm, respectively; the width and depth of the water tank are 35 mm and 45mm, respectively; the height and diameter of the embossing head column are 120mm and 70mm, respectively.

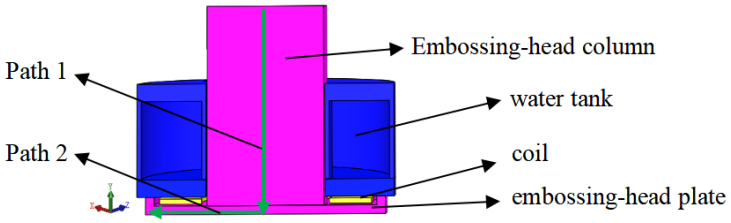

Fig. 1 The structure of the embossing head model

Due to the complex geometric structure of the embossing head, to simplify the complex problem and meet the working limit of the computer, the influence of any external factors on the embossing head can be ignored. Therefore, the following assumptions were made for the embossing head of the hot embossing machine during the modelling and problem solving processes:

(a) It is considered that the material of the structural parts is approximately uniform and isotropic;

(b) The quantities in the field are sinusoidal and change with time;

(c) All structural parts of the embossing-head are symmetrical along the centreline.

(2) Mesh generation

To boost the calculation accuracy and save the computing resources, a hexahedron mesh was realized utilizing a mapping mesh. In Figure 2, the method of mesh division used in this article is demonstrated. The number of nodes and cells in the finite element model is 15,576 and 12,591, respectively.

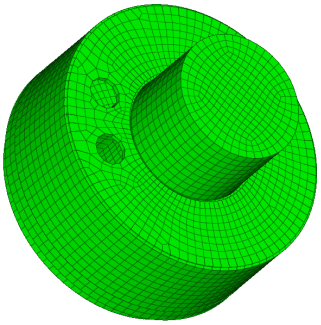

Fig. 2 A schematic diagram of grid division

(3) Setting of the material

The materials of the embossing head structural parts are selected from the Mallwell material library. The materials of the embossing head plate, water tank, embossing head column, and coil are respectively structural steel, aluminium alloy, structural steel, and copper. The specific properties of these materials are shown in Table 1.

Table 1 Properties of the embossing head materials.

Materials	Resistivity (Ω·m)	Thermal conductivity (W/m·°C)	Relative permeability (H/ms)	Density (Kg/m^3)	Specific heat capacity (J/kg·°C)
structural steel	9.78×10^{-8}	16	8000	7.9×10^3	0.50×10^3
aluminium alloy	1.4×10^{-6}	230	1	2.7×10^3	0.88×10^3
copper	1.6×10^{-8}	377	1	8.9×10^3	0.39×10^3

(4) Setting of the boundary condition

In the process of magnetic field analysis, the current excitation and phase angle are confirmed. Simultaneously, the vortex effect carrier is selected to meet the heating requirements of the hot embossing machine.

In the process of thermal field analysis, the eddy current of external load is adopted to apply the temperature load. Due to the phenomenon of heat exchange between the embossing head and the external environment, the dominating boundary condition affecting the heat transfer on the surface of embossing head is thermal convection. The heat convection equation is as follows:

$$\varphi n = -\alpha(T - T_\alpha) \tag{13}$$

where α and T_α are respectively the convection coefficient and the environment temperature. The relevant boundary conditions in the analysis of magnetic and thermal fields are set as shown in Table 2.

Table 2 Relevant boundary conditions in the analysis of magnetic and thermal fields

Current Excitation (A)	Phase Angle (°)	Carrier	Adaptive Frequency (Hz)	Convection Coefficient ($W\cdot m^{-2}\cdot °C^{-1}$)	Environment Temperature (°C)
3000	0	Embossing -head	7500/8500/9500	20	20

The eddy current density based on the frequencies of 7500Hz, 8500Hz and 9500Hz is obtained by utilizing the above parameters. Remarkably, the energy required for heat conduction is provided *via* the eddy current power of electromagnetic induction.

4. Results and Discussion

In thermoforming, different materials are usually processed at a temperature close to the glass transition temperature. In the hot embossing test, hot-pressing should be carried out at a temperature that is higher by more than 10°C than the glass transition temperature and demoulding should be carried out below the glass transition temperature to ensure that the microchannel is completely manufactured [24]. The glass transition temperature and the hot embossing temperature of three different materials are shown in Table 3 to describe the limits and requirements of parameters in the microchip replication process.

Table 3 The glass transition temperature and the hot embossing temperature of different materials.

Materials	Glass-transition Temperatures	Hot-embossing Temperatures	References
PMMA	105°C	> 115°C	[25]
PC	150°C	> 165°C	[26]
PAA	106°C	> 116°C	[27]

4.1 Distance between the Coil and the Embossing Head Plate

The inductive distance of the heating coil is a significant factor affecting the final heating efficiency. The influence of different inductive distances on the distribution of the embossing head temperature is shown in Figure 3. When the induction frequency is 1500Hz and the heating time is 300s, the temperature distributions of the embossing head plate transverse position (path 1) and embossing head column longitudinal position (path 2) are respectively discussed in distances of 0 mm, 1 mm, and 5 mm between the coil and the embossing head plate.

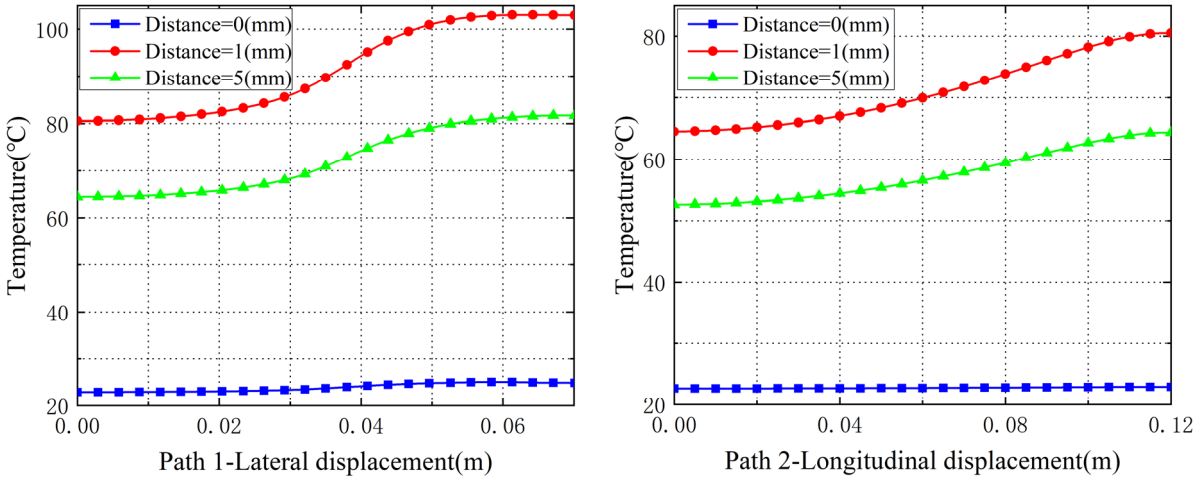

Fig. 3 The influence of coil position on temperature distribution

Noticeably, the heating temperatures on path 1 and path 2 show increasing trends, owing to the selected paths getting closer to the heating coil. Unfortunately, when the distance is 0 mm, the temperatures change slightly on path 1 and path 2, and the maximum temperature is almost close to the room temperature. At this moment, the efficiency of induction heating is almost close to 0. This phenomenon is attributed to the small distance between the coil and the embossing head plate causing no LC resonance and then a weak high-frequency current. Furthermore, the power cannot be adjusted to a higher level on the account of the weak current. Remarkably, the average value of temperature along path 1 and path 2 is highest when the distance is 1mm. Take the average temperature on path 1 as an example; compared with distances of 0mm and 5mm, the average value is boosted by 4 times and 1.5 times, respectively. The cause of this phenomenon is that the heat is produced *via* the eddy currents generated in the metallic conductors through utilizing the electromagnetic coil radiation rather than the electromagnetic coil itself. Therefore, the efficiency of electromagnetic induction heating increases with the decrease in the distance provided that the distance between the coil and the embossing head plate is not 0 mm.

Combining the analysis results with the actual demand, the distance of 1 mm between the coil and the embossing head plate is employed not only to satisfy the requirement of LC oscillation but also to enhance the thermal generation efficiency of induction heating.

4.2 Embossing Head Material

The magnetic permeability of the metal material is a crucial factor affecting heating efficiency. The influence of different magnetic permeability on the distribution of the embossing head temperature is shown in Figure 4. For the given parameters, i.e. an induction frequency of 8500Hz and a heating time of 300s, the temperature distributions of the

embossing head plate transverse position (path 1) and the embossing head column longitudinal position (path 2) are respectively deciphered under three conditions of structural steel, aluminium alloy, and copper.

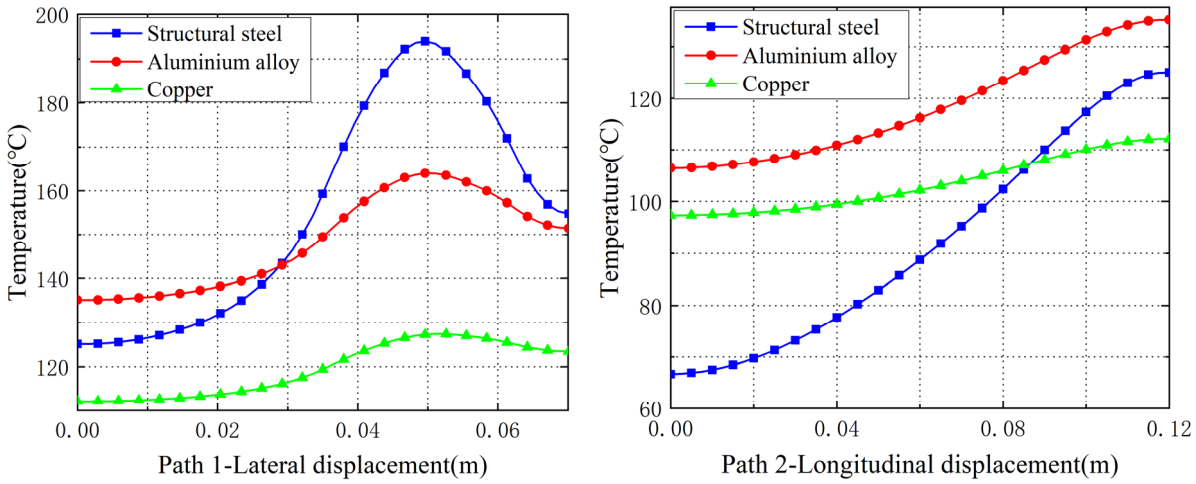

Fig. 4 The influence of head materials on temperature distribution

The heating temperature on path 1 first shows an increasing trend and then a decreasing one. Taking the aluminium alloy as an example, the temperature rises from 135℃ to 165℃ at the beginning and then falls to 150℃. The reason for the highest temperature at X=0.05mm is that the location of the selected path is first close to the coil and then further away from the coil. Therefore, the temperature increases first and then decreases. The heating temperature on path 2 shows an increasing trend due to fact that the nodes on path 2 gradually get closer to the coil. The magnetic conductivity of structural steel is the best among the three materials. In consequence, the thermal generation rate and the mean temperature are highest on path 1. Unfortunately, the maximum temperature occurs at X=0.05m and it is not located in the effective area of practical application (the region of 0m- 0.003m). For aluminium alloy, the average temperature is highest on path 2. Furthermore, this phenomenon does not satisfy the design requirements due to the higher temperature on the embossing head column. A common conclusion drawn from Figure 4 is that the slope of the average temperature of copper is the least steep in comparison with the other two materials. In other words, the heating temperature is most evenly distributed on path 1 and path 2 owing to better thermal conductivity of copper. This is most evident on the path1 effective heating area of 0m - 0.003m where the temperature variations are smallest.

Based on the analysis results and the actual demand, copper is selected as the material for the embossing head. This material can satisfy the uniformity of temperature distribution in the hot embossing process and can also boost the processing quality of the chip.

4.3 Frequency of Electromagnetic Induction Heating

The determination of the heating frequency is the key to the normal operation of the embossing head. Specifically, different induction heating frequencies have different heating characteristics. The influence of different induction heating frequencies on the embossing head temperature distribution is shown in Figure 5. For the given parameters, i.e. the embossing-head material which is copper and a heating time of 300s, the temperature distributions of the embossing head plate transverse position (path 1) and the embossing head column longitudinal position (path 2) are respectively discussed with different frequencies of 7500Hz, 8500Hz, and 9500Hz.

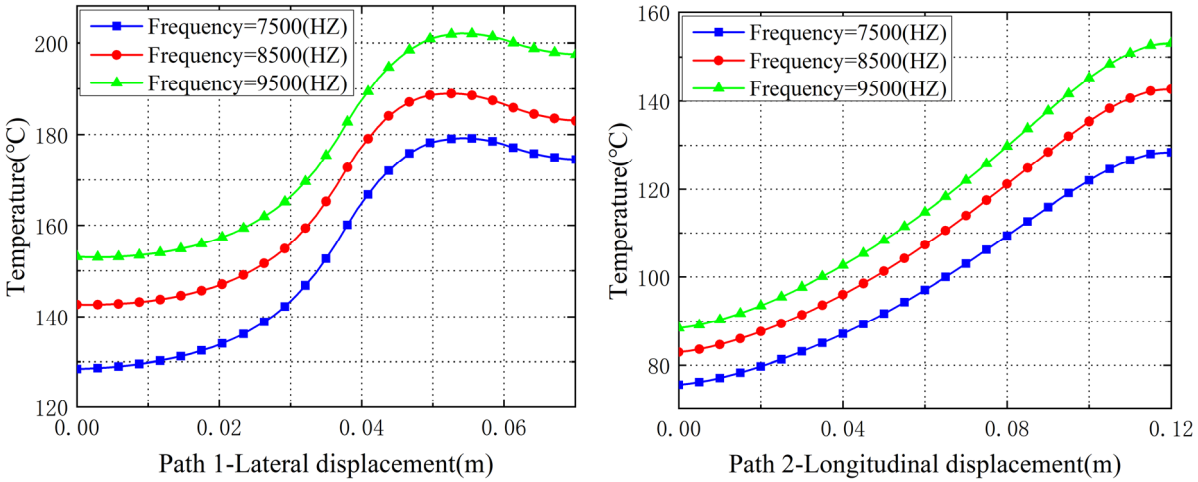

Fig. 5 The influence of frequencies on temperature distribution

It is pretty obvious that the induction heating efficiency increases with the boosts in the heating frequencies on path 1 and path 2. Taking X=0.05m on the path 1 as an example, the corresponding temperatures of the three frequencies are 180℃, 190℃, and 200℃, respectively, owing to the fact that higher frequency results in a higher degree of conversion from electric energy to magnetic energy and then to thermal energy. Taking frequencies of 7500Hz and 9500Hz on path 2 as examples, it is worth mentioning that when the frequency is 7500Hz, the low-temperature requirements of the embossing head column are satisfied due to the lowest average temperature; in addition, the highest level of heat is generated when the frequency is 9500Hz. Nonetheless, in the 0.00-0.03 mm effective heating range, the average temperatures for both frequencies are 130℃ and 155℃, respectively. Compared with the actual demanded temperature of 140℃, the temperature value is not optimal. Noticeably, the average temperature is closest to the actual requirement on the path1 effective heating area when the frequency is 8500Hz, and it only takes 10 minutes to fabricate a chip.

Combining the analysis results with the actual requirements, the frequency of 8500Hz is utilized for electromagnetic induction heating in the embossing head not only to satisfy the temperature requirement of the hot embossing replication process but also to improve the processing efficiency of the chip.

4.4 Cooling Water Velocity (Coefficient of Convection Heat Transfer)

In order to ensure the moulding quality of the chip, cooling water is utilized to reduce temperature. The cooling water velocity is replaced by convection heat transfer coefficients to study the influence of different cooling water velocities on the distribution of temperature in the embossing head, which is shown in Figure 6. For the given parameters, i.e. copper as the embossing-head material, a frequency of 8500Hz and a heating time of 300s, the temperature distributions of the embossing head plate transverse position (path 1) and the embossing head column longitudinal position (path 2) are respectively deciphered using heating transfer coefficients of 1000 ($W \cdot m^{-2} \cdot °C^{-1}$), 1200 ($W \cdot m^{-2} \cdot °C^{-1}$), and 1400 ($W \cdot m^{-2} \cdot °C^{-1}$).

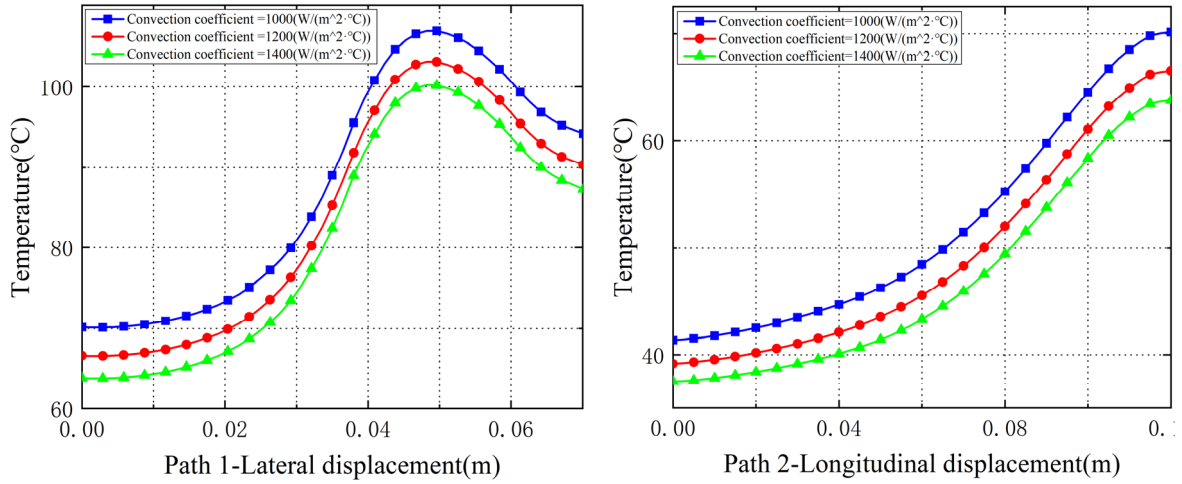

Fig. 6 The influence of convection heat transfer coefficients on temperature distribution

The analysis results demonstrate that the heating temperature on path 1 first shows an increasing trend, and then a decreasing one. The case of X=0.05mm exhibits the highest temperature. The reason for this phenomenon is that the coil is in the central location at X=0.05mm. The cooling effect is more and more noticeable with the increase in the convection heat transfer coefficients on path 1 and path 2 because the convection heat transfer coefficient is a significant factor affecting the cooling efficiency. Remarkably, when the convection heat transfer coefficient is 1400 ($W \cdot m^{-2} \cdot °C^{-1}$) in the path1 effective heating area of 0.00m-0.003m, the overall cooling effect is the strongest, compared with the other two circumstances. At this time, the average temperature is close to the temperature requirement of 60℃ in the chip demoulding. Simultaneously, when the convection heat transfer coefficient is 1400 ($W \cdot m^{-2} \cdot °C^{-1}$) on path 2, the low-temperature requirements of the embossing head column are satisfied because the average temperature of the embossing head is the lowest of all three cases.

Based on the analysis results and the actual demand, the convection heat transfer coefficient of 1400 ($W \cdot m^{-2} \cdot °C^{-1}$) is utilized; namely, the water flow velocity is 1.2 $m \cdot s^{-1}$. This method not only satisfies the temperature requirements of cooling and demoulding in the hot-embossing replication process but also guarantees the processing quality of the chip.

4.5 Comparing Different Embossing Heads for Heating

The heating parameters of embossing heads utilizing different heating methods are listed in Table 4. In terms of meeting the demand, all three types of embossing heads can meet the requirements of hot embossing temperature. Nonetheless, for the resistance wire heating [28], there are many insufficiencies including low heat transfer efficiency and short service life, and the heating rate is the lowest compared with the other two heating methods. Remarkably, for the thermoelectric refrigeration reactor [29], some heating parameters, such as the heat transfer efficiency and heating rate, and service life are improved compared with the resistance wire heating. However, when this method is used, 30% of the heat is not utilized efficiently [29]. Fortunately, the electromagnetic induction heating technology of embossing head is presented in this paper to avoid the problems of low heat transfer efficiency, low heating rate, and short life. In summary, the embossing head using electromagnetic induction heating meets all the requirements discussed in this paper and it has advantages of high efficiency, high heating rate, and long life.

Table 4 Comparison of heating parameters of different embossing heads.

Object	Heating method	Meet the demand	Heat transfer efficiency	Heating rate	Useful life
The embossing head from [28]	Resistance wire heating	Yes	40%	25℃/min	Short
The embossing head from [29]	Thermoelectric refrigeration reactor	Yes	70%	30℃/min	Ordinary
The embossing head of this paper	Electromagnetic induction heating	Yes	95%	112.5℃/min	Long

The advantages of electromagnetic induction heating are described in this paper; to further highlight the characteristics, the dynamic responses of different heating methods are compared, as shown in Figure 7.

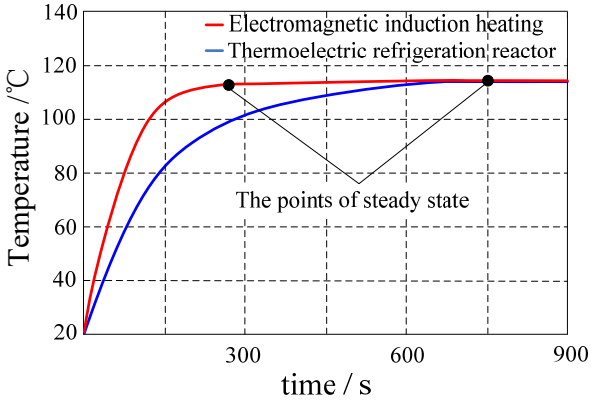

Fig. 7 The dynamic response of different heating methods

Take the 115 ℃ temperature required for a PMMA hot-embossing as an example. It can be clearly seen from the figure above that for the same temperature requirement the speed of electromagnetic induction heating is faster. Furthermore, for the two heating methods, the time for electromagnetic induction to reach a steady-state (about 250s) is three times shorter than that in the thermoelectric refrigeration reactor (about 750s).

5. Concluding Remarks

In this study, an embossing head utilizing electromagnetic induction heating is employed to boost the performance of the hot embossing machine. Based on the ANSYS/Workbench, numerical simulation and analysis are performed to investigate the influence of the coil distribution position, material of embossing head, heating frequency, and cooling water velocity on the temperature distribution in the embossing head. The study shows that the heating efficiency increases with a decrease in the distance provided that the distance between the coil and the embossing head plate is not 0 mm; the heating temperature is most evenly distributed on path 1 and path 2 owing to the copper possessing better thermal conductivity; the average temperature is closest to the actual requirement in the path1 effective heating area when the frequency is 8500Hz and, compared with the other two circumstances, the cooling effect is the best when the convection heat transfer coefficient is 1400 ($W \cdot m^{-2} \cdot ℃^{-1}$). Consequently, for the following parameters, i.e. a distance of 1 mm between the coil and the embossing head, copper as the material, a frequency of 8500 Hz, and a water velocity of 1.2 $m \cdot s^{-1}$, the hot embossing machine temperature requirements are satisfied, including the hot embossing and the demoulding process. Simultaneously, the processing time of the chips when this embossing head is used has been reduced from

30 minutes to 10 minutes, compared with the existing heating methods of embossing heads. In summary, the embossing head which meets all the requirements in this paper has advantages of high efficiency, high heating rate, and long life. Next, this embossing head will be utilized to carry out related hot embossing experiments.

REFERENCES

[1] Jiang, H.; Lv, X.F.; Zhao, K.X. Progress of Aptamer Screening Techniques Based on Microfluidic Chips. Journal of Analytical Chemistry. 2020, 48(5): 590-600. https://doi.org/10.1016/S1872-2040(20)60015-9

[2] Lu, S.S.; Dugan, C.E.; Kennedy, R.T. A microfluidic chip with integrated electrophoretic immunoassay for investigating cell-cell interactions. Anal. Chem. 2018, 90: 5171-5178. https://doi.org/10.1021/acs.analchem.7b05304

[3] Zhou, L.; Chen, Y.H.; Fang, X.E.; Liu, Y.H.; Du, M.K.; Lu, X.D.; Li, Q.N.; Sun, Y.; Ma, J.Y.; Lan, T. Microfluidic-RT-LAMP chip for the point-of-care detection of emerging and re-emerging enteric coronaviruses in swine. Analytica Chimica Acta. 2020, 1125: 57-65. https://doi.org/10.1016/j.aca.2020.05.034

[4] Jo, Y.N.; Santhoshkumar, P.; Prasanna, K.; Vediappan, K.; Lee, C.W. Improving self-discharge and anti-corrosion performance of Zn-air batteries using conductive polymer-coated Zn active materials. Journal of Industrial and Engineering Chemistry. 2019 76: 396-402. https://doi.org/10.1016/j.jiec.2019.04.005

[5] Yu, Y.S.; Wang, M.C.; Zhu, Y.Q.; Zhou, J.Z.; Zhou, A. Evaporative deposition of mono-and bi-dispersed colloids on a polydimethylsiloxane (PDMS) surface. Chemical Hemical Engineering Science. 2019, 205: 212-219. https://doi.org/10.1016/j.ces.2019.05.006

[6] Kim, S.H.; Lee, S.; Ahn, D.; Park, J.Y. PDMS double casting method enabled by plasma treatment and alcohol passivation. Sensors and Actuators B-Chemical. 2019, 293: 115-121. https://doi.org/10.1016/j.snb.2019.04.145

[7] Huang, Y.J. Effect of surface treatment on surface characteristics of carbon fibers and interfacial bonding of PMMA resin composites. Composite Interfaces. 2019, 26: 679-686. https://doi.org/10.1080/09276440.2018.1526593

[8] Peng, L.F.; Wu, H.; Shu, Y.Y.; Yi, P.Y.; Deng Y.J.; Lai X.M. Roll-to-roll hot embossing system with shape preserving mechanism for the large-area fabrication of microstructures. Review of Scientific Instruments. 2016, 87(10): 013001-358. https://doi.org/10.1063/1.4963907

[9] Zhang, F.L.; Zhu J. The study of hot embossing and bonding machine for microfludic chips fabrication. Advanced Materials Research, 2011, 328-330(3): 120-123. https://doi.org/10.4028/www.scientific.net/AMR.328-330.120

[10] Wang, J.; Yi, P.Y.; Deng, Y.J; Peng, L.F.; Lai, X.F.; Ni, J. Recovery behavior of thermoplastic polymers in micro hot embossing process. Journal of Materials Processing Technology. 2017, 243: 205-216. https://doi.org/10.1016/j.jmatprotec.2016.12.024

[11] Mohammed, A.G.; Ozgur, G.; Sevkat, E. Electrical resistance heating for deicing and snow melting applications: Experimental study. Cold Regions Science and Technology. 2019, 160: 128-138. https://doi.org/10.1016/j.coldregions.2019.02.004

[12] Li, J.M.; Liu, C.; Ke, X.; Xu Z.; Li M.; Duan Y.J.; Fan Y. Wang Li-ding. Fabrication of a thermoplastic multilayer microfluidic chip. Journal of Materials Processing Technology. 2012, 212(11): 2315-2320. https://doi.org/10.1016/j.jmatprotec.2012.06.022

[13] Yamina, Z.; Khadidja Y.E.; Mohamed, K.; Nadji, M.M. A new approach for pectin extraction: Electromagnetic induction heating. Arabian Journal of Chemistry. 2017, 10: 480-487. https://doi.org/10.1016/j.arabjc.2014.11.011

[14] Li, G.; Liu, Z.Q.; Li, W.M; Lu, G.L. Electromagnetic induction heating technology in the application and research of extrusion system. Natural Science Edition. 2018, 38: 304-306.

[15] Song, W.N. Development and application of heating system on injection moulding machine based on electromagnetic heating. Science and Technology Vision. 2016, (06): 208+227.

[16] Zhang, X.Y. Improvement of heating method for plastic mould. Science and Technology Consulting Herald. 2007, (23): 212-213.

[17] Chen, W.; Wu, G.C.; Li, Y.; Ma, J. Coupled magnetic-thermal fields analysis using an adaptive single-mesh method. International Journal of Applied Electromagnetics and Mechanics, 2020, 62(1): 45-57. https://doi.org/10.3233/JAE-180093

[18] Cheng, Q.; Zhang, Z.D.; Guo, H. Simulation and analysis on electro-magnetic-thermal coupling of solenoid GDI injector. International Journal of Applied Electromagnetics and Mechanics, 2014, 46(4): 775-792. https://doi.org/10.3233/JAE-141973

[19] Li, H.J.; Zhao Y. Finite element analysis of cross helical gear transmission based on ANSYS workbench. Applied Mechanics and Materials, 2012, 189: 406-410. https://doi.org/10.4028/www.scientific.net/AMM.189.406

[20] Li, Z.Y.; Hu, Z.Q.; Lin, Gao.; Zhong, H. A modified scaled boundary finite element method for dynamic response of a discontinuous layered half-space. Applied Mathematical Modelling, 2020, 87: 77-90. https://doi.org/10.1016/j.apm.2020.05.028

[21] Wu, S.Y.; Xu, L.; Xiao, L. Air purification and thermal performance of photocatalytic-Trombe wall based on multiple physical fields coupling, Renewable Energy, 2020, 148: 338-348. https://doi.org/10.1016/j.renene.2019.10.039

[22] Tan,H.; Zhang, Y.X.; Liu, Y.X.; Fu, X.Q. ANSYS Workbench simulation of glass welding by femtosecond laser pulses. Infrared Physics & Technology, 2019, 98: 334-340. https://doi.org/10.1016/j.infrared.2019.03.036

[23] Petit, M.; Avenas, Y.; Kedous-Lebouc, A.; Cherief, W.; Rullière, E. Experimental study of a static system based on a magneto-thermal coupling in ferrofluids. International Journal of Refrigeration, 2014, 37: 201-208. https://doi.org/10.1016/j.ijrefrig.2013.09.011

[24] Xu, M.; Luo, Y.; Wang, X, D.; Li, N.; Liu, C. Finite element analysis of temperature effect in polymer hot embossing. Chinese Journal of Sensors and Actuators, 2006, 19 (5): 2015-2017.

[25] Yuang, Y.J.; James L.L.; Kurt, W.K. Hot embossing in microfabrication. Part I: experimental, Polymer Engineering and Science, 2002, 42 (3): 539-550. https://doi.org/10.1002/pen.10970

[26] Yuang, Y.J.; James L.L.; Kurt, W.K. Koelling. Rheological analysis of polyvinyl butyral near the glass transition temperature. Polymer Engineering and Science, 2001, 41(2): 275-292. https://doi.org/10.1002/pen.10727

[27] An, Y.X.; Singh, S.; Bejagam, K.K.; Deshmukh, S.A. Development of an accurate coarse-grained model of poly(acrylic acid) in explicit solvents, Macromolecules, 2020, 52(13): 4875-4887. https://doi.org/10.1021/acs.macromol.9b00615

[28] Chang, Y.K.; Hong, F.C.N. The fabrication of Zn0 nanowire field-effect transistors combining dielectrophoresis and hot-pressing. Nanotechnology, 2009, 20 (23): 235202. https://doi.org/10.1088/0957-4484/20/23/235202

[29] Wang, X.D.; Liu, C.; Wang, L.D. Development of hot-embossing machines for fabrication of polymer microstructures. China Mechanical Engineering, 2005, 16(14): 1229-1232.

Submitted: 06.10.2019

Accepted: 09.8.2021

Jun-yao Wang *
Qi Hou
Fu-wang Wang
School of Mechanical Engineering, Northeast Electric Power University, Jilin 132012, China
Bo You
School of Aeronautical Engineering, Ji Lin Institute of Chemical Technology, Jilin 132012, China
Heng-yi Yuan
College of mechanical engineering, Ji lin engineering normal University, Changchun 130052 Jilin, China
*Corresponding author:
junyao_0001@126.com